Lateral diffusion in an archipelago

Single-particle diffusion

Michael J. Saxton

Institute of Theoretical Dynamics, University of California, Davis, California 95616; and Laboratory of Chemical Biodynamics, Lawrence Berkeley Laboratory, University of California, Berkeley, California 94720 USA

ABSTRACT Several laboratories have measured lateral diffusion of single particles on the cell surface, and these measurements may reveal an otherwise inaccessible level of submicroscopic organization of cell membranes. Pitfalls in the interpretation of these experiments are analyzed. Random walks in unobstructed systems show structure that could be interpreted as free diffusion, obstructed diffusion, directed motion, or trapping in finite domains. To interpret observed trajectories correctly, one must consider not only the trajectories themselves but also the probabilities of occurrence of various trajectories. Measures of the asymmetry of obstructed and unobstructed random walks are calculated, and probabilities are evaluated for random trajectories that resemble either directed motion or diffusion in a bounded region.

INTRODUCTION

New techniques of microscopy have made it possible to observe the motion of individual proteins or small clusters of lipids on the cell surface (2, 9, 11, 18, 19, 25, 28, 43). These techniques provide a powerful tool to characterize submicroscopic domain structure in biological membranes. In these experiments, proteins or lipids are labeled with a highly fluorescent label or with colloidal gold microspheres. Computer-enhanced video microscopy is used to track the trajectory of individual particles as they move on the cell surface. The time resolution is typically 1/30 s and the spatial resolution is 5–50 nm. The shape of the trajectories suggests various biologically important processes, such as binding to immobile species, free diffusion, hindered diffusion, directed transport, and trapping of particles in bounded microdomains. Transitions between these types of motion are observed.

Unfortunately these trajectories can also occur, with distressingly high probability, in random walks in an unobstructed system. To interpret the observed trajectories, one must consider not only the trajectories themselves but also the probability of occurrence of various trajectories in obstructed and unobstructed systems. It is necessary to use the proper control (5, 6): a two-dimensional unobstructed random walk. This problem has been recognized in the literature, but there have been few tools available to solve it. The general problem is complicated, so this paper will focus on two special cases, directed transport, and trapping in bounded domains.

These special cases are biologically significant. Identifying directed motion is essential in studies of the mechanism of cellular locomotion (25) and the interaction of membrane proteins with the cytoskeleton (31). Trapping in domains may have a major influence on reaction kinetics (23, 26, 27), and equilibrium (48). Diffusion may be restricted by gel-phase lipids (49), the cytoskeleton (2, 9, 47), the membrane skeleton (41), or the extracellular matrix (51); any of these obstacles could trap mobile species in domains. Domain structure in membranes was recently reviewed (10, 22).

Little work has appeared in the biophysics literature on the theory of single-particle diffusion measurements, except for the recent paper by Qian et al. (35), emphasizing the statistical accuracy of the measurements. Some work on the shape of random walks has appeared in the physics literature, often emphasizing random walks in high dimensions (38). Much work has appeared in the polymer literature on random walks and self-avoiding walks as models of polymer conformation (4, 17, 44, 45). Little, if any, of this work has included the effects of obstructions. The work presented here is inspired in part by the work of Bookstein (5, 6) pointing out that one-dimensional random walks are the proper control for time sequences of morphological change in evolution. The theory of random walks was reviewed by Weiss and Rubin (50).

The paper is organized as follows. First, some examples of unobstructed random walks are given, to show that there is in fact a problem. Next, the displacement of a diffusing particle is characterized by histograms of the displacement at fixed times. Then, two parameters are used to show the asymmetry of random walks. Finally, methods are proposed to determine whether an observed trajectory is a result of directed motion or diffusion, and whether a diffusing particle is in a bounded region. Both unobstructed and obstructed random walks are considered. The obstacles consist of random points, cluster–cluster aggregates, and point obstacles arranged to produce a bounded domain, usually hexagonal.

METHODS

Diffusion calculations are carried out as described earlier (39, 42). A 256×256 triangular lattice is used, with periodic boundary conditions. Point obstacles are placed on the lattice at random. A tracer is placed at a random unblocked point on the lattice, and carries out a random walk on unobstructed lattice sites. The calculation is repeated for

Address correspondence to Dr. Michael J. Saxton, Institute of Theoretical Dynamics, University of California, Davis, CA 95616-8618, USA.

0006-3495/93/06/1766/15 $2.00

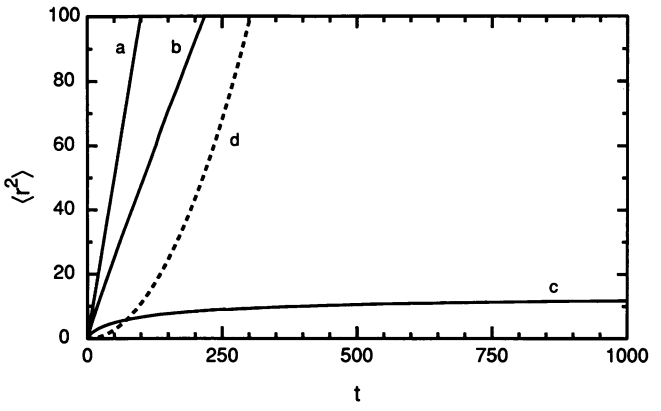

FIGURE 1 Mean-square displacement $\langle r^2 \rangle$ as a function of time t for different types of motion (40). This is based in part on a figure of Sheetz et al. (43). The protein diffusion coefficient is taken to be $D_0 = 3 \times 10^{-11}$ cm^2/s, and the velocity $v = 20$ nm/s, as in reference 43. For a sampling time $\tau = 33$ ms, then, $\ell = 20$ nm from Eq. 3c. In dimensional units, the range of the x-axis is 33 s and that of the y-axis, 0.040 μm^2. (Curve a) Random walk on a triangular lattice with no obstructions. (Curve b) Random walk with an area fraction of random point obstacles of $C = 0.3$. (Curve c) Random walk with an area fraction of random point obstacles of $C = 0.65$, above the percolation threshold of 0.5 for a triangular lattice. (Curve d) Directed motion, for which $\langle r^2 \rangle = v^2 t^2$.

various starting positions of the tracer within a given configuration of obstacles, and various configurations of obstacles at the same concentration. Typically 100 different configurations of obstacles were used, and 1000 different tracers within each configuration of obstacles. At each time step, the position of the tracer is obtained, and the sums required for the radius of gyration tensor are recorded. At prescribed times, histograms of the displacement and the largest displacement are compiled, the radius of gyration tensor is diagonalized, and histograms of the asymmetry parameters are compiled. Error limits for the histograms are discussed in the captions. For values of the diffusion coefficient D^*, independent runs gave results reproducible to 1.5% in the worst case, and 0.2–0.5% typically.

Cluster–cluster aggregates are constructed by standard methods (24, 30), as described in detail elsewhere (42). Initially, particles are placed on randomly chosen sites at a prescribed concentration. Adjacent particles are assumed to form clusters, and isolated particles form clusters of unit mass. The clusters then carry out a random walk. Whenever two clusters become adjacent, they are merged into a rigid cluster irreversibly, with probability one. They move as a unit thereafter, with a translational diffusion coefficient inversely proportional to mass. The random walk continues until only one cluster remains, the final cluster-cluster aggregate.

RESULTS

Trajectories of random walks

We consider trajectories obtained from Monte Carlo calculations. In these calculations, lattice sites are blocked at random, and the obstacle concentration is given as an area fraction C, equal to the fraction of blocked sites. A point tracer carries out a random walk on unblocked sites of the lattice, and its displacement from its starting position is recorded at prescribed times, yielding the displacement r^2 as a function of time t. Displacements are averaged over different random starting points within a given configuration of obstacles, and different random configurations of obstacles at the prescribed area fraction. This averaging yields the mean-square displacement $\langle r^2 \rangle$ as a function of t. In the usual Monte Carlo calculations (12, 34, 39, 40, 42), the diffusion coefficient is obtained from the mean-square displacement, but here we focus on individual trajectories and the probability of their occurrence.

At low concentrations of obstacles, the mean-square displacement is

$$\langle r^2 \rangle = 4Dt. \tag{1}$$

The observed diffusion coefficient D is written in terms of the diffusion coefficient D_0 in the absence of obstacles and a dimensionless, concentration-dependent diffusion coefficient $D^*(C)$:

$$D = D_0 D^*(C), \tag{2}$$

with $D^*(0) = 1$. The Monte Carlo calculations are carried out in dimensionless units

$$r^* = r/\ell, \tag{3a}$$

$$t^* = t/\tau, \tag{3b}$$

where ℓ is the lattice spacing and τ is the jump time, related by

$$\ell^2 = 4D_0\tau. \tag{3c}$$

The dimensionless mean-square displacement is then

$$\langle r^{*2} \rangle = D^*(C)t^*. \tag{4}$$

To simplify the notation, the asterisks are dropped unless it is necessary to distinguish the dimensional and dimensionless variables.

The usual way of analyzing a random walk is to plot the mean-square displacement as a function of time, to obtain curves as shown in Fig. 1. These are averaged over ≥5000 trajectories. Unobstructed diffusion yields a straight line of unit slope, giving $D^* = 1$ (curve a). Diffusion in the presence of low concentrations of random point obstacles gives, at large times, a straight line of slope < 1, corresponding to $D^* < 1$ (curve b). At high concentrations of random point obstacles, the system is above the percolation threshold, so that there are no long-range paths for diffusion. The diffusing particles are

TABLE 1 **Diffusion coefficients as a function of obstacle concentration**

	C	D^*
Obstacles	0.0	0.999
	0.1	0.819
	0.2	0.629
	0.3	0.425
	0.4	0.210
Cluster–cluster aggregates	0.1	0.316
	0.3	0.0840

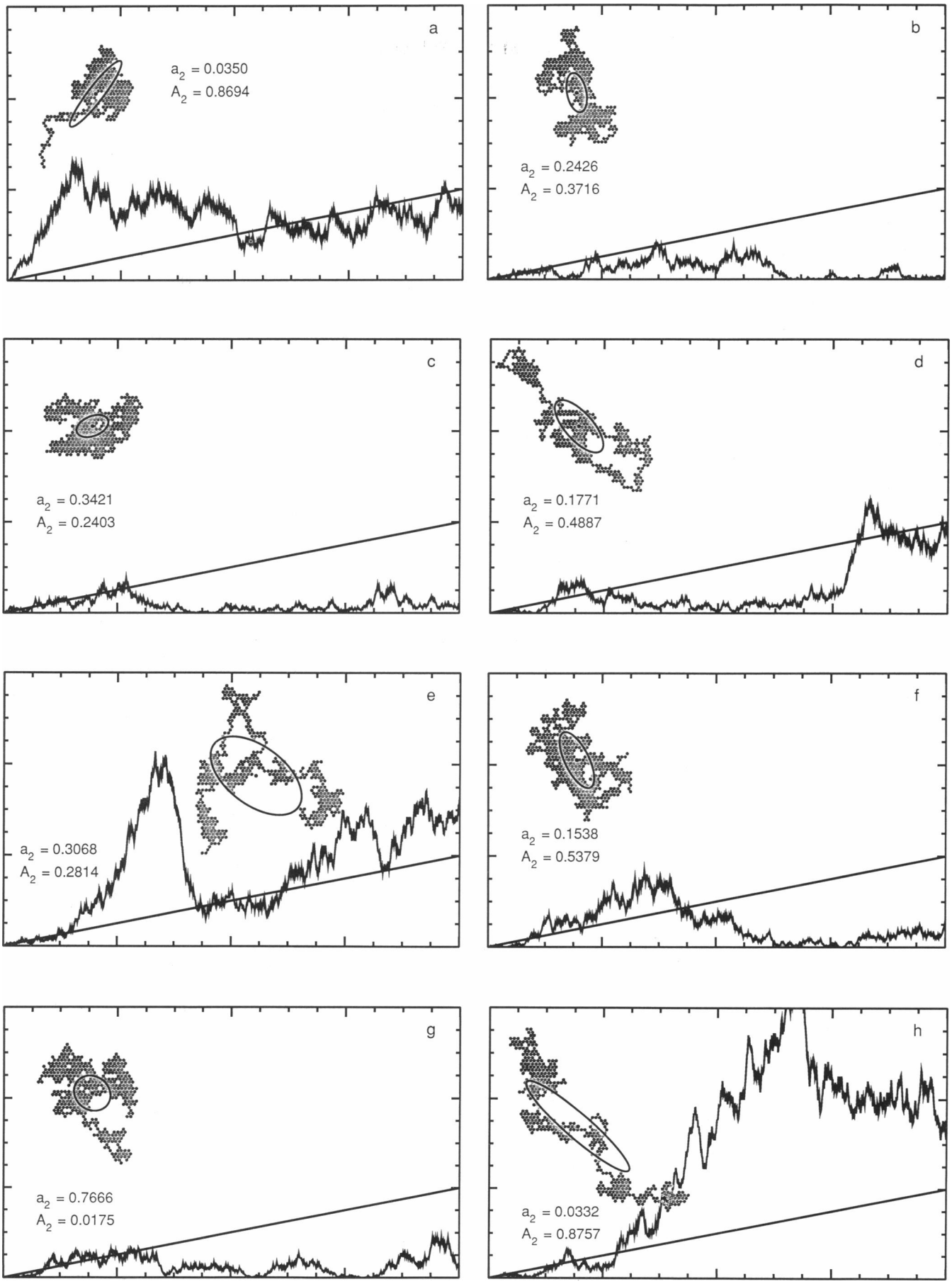
a
a_2 = 0.0350
A_2 = 0.8694
b
a_2 = 0.2426
A_2 = 0.3716
c
a_2 = 0.3421
A_2 = 0.2403
d
a_2 = 0.1771
A_2 = 0.4887
e
a_2 = 0.3068
A_2 = 0.2814
f
a_2 = 0.1538
A_2 = 0.5379
g
a_2 = 0.7666
A_2 = 0.0175
h
a_2 = 0.0332
A_2 = 0.8757

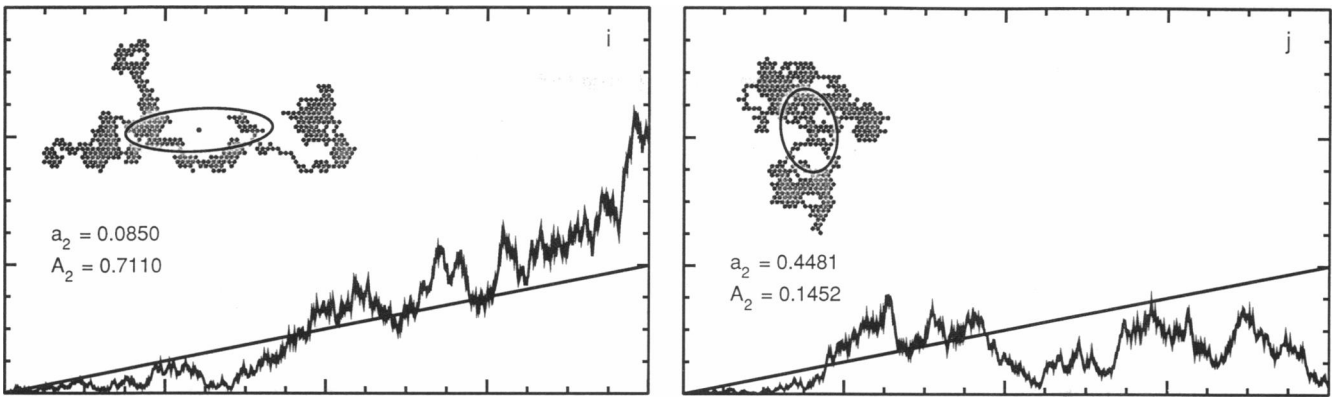

FIGURE 2 Displacement r^2 as a function of time t (in dimensionless units) for a sequence of 10 random walks on an unobstructed triangular lattice. To save space, scales are not shown. The x-axis corresponds to 1024 time steps; major divisions are 256 units. The y-axis corresponds to $r^2 = 3072$; major divisions are 1024 units. The straight line is $\langle r^2 \rangle = t$, the mean-square displacement in dimensionless units averaged over a large number of random walks. For each random walk, a map of the distinct sites visited by the tracer is shown, along with the center of mass of the random walk (*filled circle*), the ellipse of gyration, and the asymmetry parameters a_2 and A_2, all discussed later.

trapped in bounded domains, so that $\langle r^2 \rangle$ levels off at large values of t, and the limiting value $\langle r^2(\infty) \rangle$ is a measure of the size of the domains (curve *c*). In directed transport, the observed species is attached to mobile cytoskeletal elements or is carried along in a bulk membrane flow. The tracer moves in a nondiffusive manner according to $r = vt$, where v is velocity (curve *d*).

Data analysis requires a value of D. To interpret Monte Carlo data, dimensionless variables are used (Eqs. 1–4). Table 1 gives values of D^* obtained from Monte Carlo calculations and Eq. 1 for various concentrations of obstacles. To interpret experimental data, dimensional variables are used. The value of D used ought to be an average value, obtained from fluorescence photobleaching recovery measurements, or from single-particle diffusion measurements averaged over a large number of trajectories.

Fig. 1 shows averages over a large number of trajectories; Fig. 2 shows a sequence of 10 individual random walks. In Fig. 2, r^2 is given as a function of time t; the irregular blobs are maps of the sites visited by the tracer. Note the apparent structure. Fig. 2 *i* and the first part of Fig. 2 *a* suggest free diffusion, at much different rates; Fig. 2, *b, c,* and *g* suggests trapping in a bounded region; Fig. 2 *d* suggests diffusion in a bounded region followed by a period of rapid motion, perhaps directed transport. Yet all these are purely random walks, with no obstacles whatsoever, and no mechanism for directed motion. Note the frequency of random walks with apparent structure. This is not a pathological set of random walks selected to show extremes, but a typical sequence generated by the Monte Carlo program.

A random walk has no characteristic time scale, and the fluctuations seen in Fig. 2 appear on all time scales (16). Fig. 3 shows a single random walk on an unobstructed lattice at three different time scales. The random walk is self-similar; there is no change in appearance as the random walk is magnified, until individual steps on the lattice can be seen. Self-similarity was noted by Perrin in measurements of Brownian motion published in 1909 (see reference 29). But if there are obstacles with structure on some length scale, the random walk will show structure on the corresponding time scale.

Distribution of displacements

One method of analyzing single-particle diffusion measurements uses histograms of the displacement at various fixed times (2). The solution of the diffusion equation in two dimensions for an instantaneous point source at the origin at a time $t = 0$ is (reference 8, p. 258)

$$C(r, t) = \frac{1}{4\pi Dt} \exp(-r^2/4Dt), \tag{5}$$

where $C(r, t)$ is the concentration and D is the diffusion coefficient. The probability density is

$$P(r, t)dr = 2\pi r dr C(r, t), \tag{6}$$

and the mean-square displacement is

$$\langle r^2(t) \rangle = \int_0^\infty 2\pi r \, dr C(r, t) r^2 = 4Dt, \tag{7}$$

so that

$$P(r, t)dr = \frac{2rdr}{\langle r^2(t) \rangle} \exp[-r^2/\langle r^2(t) \rangle]. \tag{8}$$

The probability that a particle has diffused a distance r_0 or greater at a time t is

$$\Pr(r \geq r_0) = \int_{r_0}^\infty P(r, t) \, dr = \exp[-r_0^2/\langle r^2(t) \rangle]. \tag{9}$$

This equation provides one test for directed motion.

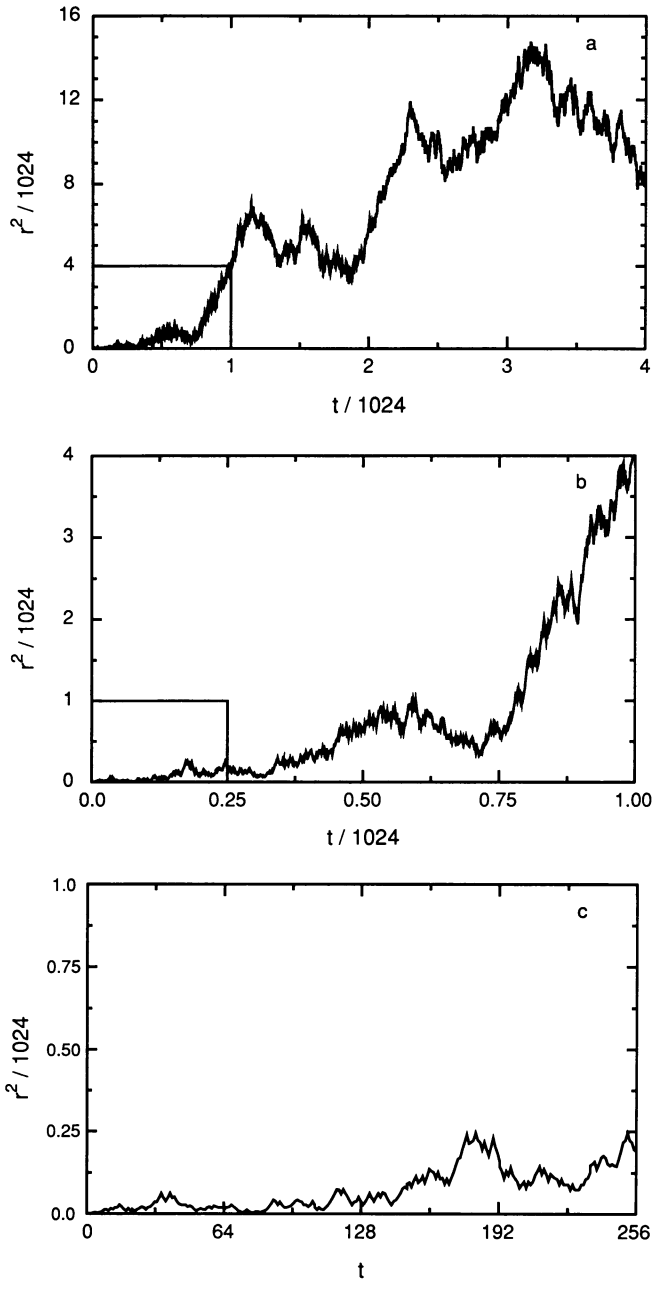

FIGURE 3 Displacement r^2 as a function of time for one random walk (in dimensionless units) on an unobstructed lattice at three different time scales. The boxes in *a* and *b* show the portion of the random walk enlarged in the next graph. Both scales change by a factor of 4 in each enlargement.

In Fig. 4, Monte Carlo results are compared with Eq. 8. Consider the results when long-range diffusion is allowed. Fig. 4 *a* shows $P(r, t)dr$ for unobstructed diffusion from Eq. 8, and two sets of data points from Monte Carlo calculations. Agreement is good, with deviations resulting from statistical noise, binning, and the discrete structure of the lattice. Fig. 4 *b* shows similar curves and Monte Carlo data for random point obstacles at an area fraction $C = 0.3$, with D^* from Table 1. With this value of D^*, Eq. 8 describes the Monte Carlo results well. At moderate concentrations, random point obstacles decrease the rate of diffusion but do not change the shape of the probability distribution. But if the tracers are obstructed by a cluster–cluster aggregate at the same area fraction, Eq. 8 does not fit the data well, because the positions of the obstacles are correlated, not random (42). Fig. 4 *c* shows Monte Carlo results for the aggregate, and curves from Eq. 8 with D^* from Table 1.

When long-range diffusion is blocked, the behavior of the curves changes. At $C = 0.5$, the percolation threshold for the triangular lattice, Eq. 8 is not applicable. Monte Carlo results are shown in Fig. 4 *d*. At this concentration of obstacles, some tracers are on percolating clusters and have long-range diffusion paths open to them; the probability distribution for these tracers follows a generalization of Eq. 8 (21). Other tracers are trapped in finite clusters, and yield a different probability distribution. The observed $P(r, t)$ is an average of these distributions. The persistent peak at low R is due to trapped tracers. At $C = 0.6$, all the tracers are trapped in finite clusters, and the probability density reaches a limiting value with time, as shown in Fig. 4 *e*. Similarly, for tracers trapped in a hexagon of radius 15, the probability density reaches a limiting value, as shown in Fig. 4 *f*, but the shape of the limiting distribution is different, reflecting the different sizes and shapes of the domains.

Asymmetry of random walks

The average behavior of a diffusing particle is symmetric: a Gaussian distribution growing shorter and wider with time (Eq. 5). But the random walks making up that average tend to be highly asymmetric, simply because there are many more asymmetric conformations than symmetric ones (37). In this section we consider two parameters that characterize the asymmetry of random walks, and use them to show that asymmetry is the rule, not the exception. These measures of asymmetry are useful in recognizing directed motion, because directed motion produces a very elongated trajectory. The asymmetry of random walks was reviewed by Rudnick and Gaspari (38).

For a random walk of n steps, the two-dimensional radius of gyration tensor is (38, 45)

$$\mathbf{T} = \begin{pmatrix} \langle x^2 \rangle - \langle x \rangle^2 & \langle xy \rangle - \langle x \rangle \langle y \rangle \\ \langle xy \rangle - \langle x \rangle \langle y \rangle & \langle y^2 \rangle - \langle y \rangle^2 \end{pmatrix}, \quad (10)$$

where the averages are over all n steps in the random walk: $\langle x \rangle = (1/n) \sum_{i=1}^{n} x_i$, and so forth. This tensor can be diagonalized by a rotation through an angle

$$\phi = \frac{1}{2} \tan^{-1} \left(\frac{2T_{xy}}{T_{xx} - T_{yy}} \right). \quad (11)$$

The principal radii of gyration are the eigenvalues of the tensor $\mathbf{T}$,

$$R_1^2, R_2^2 = {}^1/_2[(T_{xx} + T_{yy}) \pm \sqrt{(T_{xx} - T_{yy})^2 + 4T_{xy}^2}], \quad (12)$$

and the radius of gyration is

$$R_G^2 = R_1^2 + R_2^2. \quad (13)$$

One way to illustrate the asymmetry of the trajectory is the ellipse of gyration, an ellipse of semiaxes R_1 and R_2, oriented at an angle ϕ, and centered on the center of mass of the trajectory. Examples are given in Fig. 2.

One measure of asymmetry is the ratio of the smaller to the larger principal radius of gyration (15),

$$a_2 = R_2^2/R_1^2. \quad (14)$$

Linear trajectories have $a_2 = 0$; circularly symmetric trajectories have $a_2 = 1$. Note that the averages in **T** are sums over the position at each time point, and are properties of a trajectory, not of the distinct sites visited. Consider three unblocked points forming an equilateral triangle, A at (0, 0), B at (1, 0), and C at ($^1/_2$, $\sqrt{3}/2$), with all adjacent points blocked. Two different trajectories with the same points visited and the same endpoints, say ABCABC and AAAABC, have different values of $\langle x \rangle$, $\langle y \rangle$, · · · and therefore different asymmetry parameters, here $a_2 = 1$ and $a_2 = {}^1/_2$, respectively.

The eigenvalue ratio a_2 is useful in distinguishing directed motion from diffusion, but not in resolving the structure of different types of obstacles. Fig. 5 shows histograms of a_2. For unobstructed diffusion and diffusion with random point obstacles below the percolation threshold, the curve rapidly converges to a time-independent value, as shown in Fig. 5 *a*. Both R_1^2 and R_2^2 increase with time, but their ratio quickly becomes time independent. Below the percolation threshold, the curve is independent of obstacle concentration, as shown in Fig. 5 *b* for $C = 0.0$–0.4. But, as the concentration of obstacles approaches the percolation threshold, the shape of the curve changes, as shown in Fig. 5 *b* for $C = 0.5$. (Changes in shape are apparent at the peak of the curve for $C = 0.45$ but not for $C = 0.40$.) For diffusion in a finite region, the curve is strongly time dependent, as shown in Fig. 5 *c* for a hexagonal domain of radius 7. Initially the probability distribution resembles the curve for an unobstructed random walk, but as time increases the curve shifts to a form reflecting the shape of the domain. Fig. 5 *d* compares the histograms for diffusion in the presence of random point obstacles and cluster-cluster aggregates at an area fraction of 0.3. The aggregates are much more effective obstacles than random points are (42); the diffusion coefficients are $D^* = 0.425$ for random points and $D^* = 0.0840$ for aggregates. Despite this difference in D^*, the histograms are similar, indicating that a_2 is not a sensitive probe of obstacle structure.

What this parameter shows is that asymmetry is common. There are few linear or circularly symmetric trajectories. For diffusion in the presence of random point obstacles below the percolation threshold, the average value is $\langle a_2 \rangle = 0.28$, corresponding to $R_2/R_1 = 0.53$, and the most probable value is $a_2 = 0.12$, corresponding to $R_2/R_1 = 0.35$. Random walks are less symmetric than percolation clusters, for which $\langle a_2 \rangle = 0.4$ (15).

Another measure of asymmetry is the parameter (36, 38)

$$A_2 = \frac{(R_1^2 - R_2^2)^2}{(R_1^2 + R_2^2)^2}. \quad (15)$$

The numerator measures the deviation from circularity; the denominator normalizes the deviation by the radius of gyration. This parameter is equal to 0 for circularly symmetric trajectories and 1 for linear trajectories. Rudnick and Gaspari (38) emphasize one average, $\langle (R_1^2 - R_2^2)^2 \rangle / \langle (R_1^2 + R_2^2)^2 \rangle$, for which they obtain an analytic form for high dimensions, but they consider $\langle A_2 \rangle$ to be the better parameter to characterize a random walk.

Histograms of A_2 show little time dependence when the obstacle concentration is below the percolation threshold. Below the threshold, the histogram is again independent of the obstacle concentration, as shown in Fig. 6. (Again, concentration dependence is apparent at $C = 0.45$ but not at $C = 0.40$.) As C increases, the fraction of points with $A_2 = 1$ increases; these result from tracers trapped on isolated points and pairs of points. Although a_2 and A_2 are trivially related for any individual trajectory, their averages over a set of trajectories are not.

The histograms of A_2 are in excellent agreement with those obtained for a random polymer by Brownian dynamics calculations for a ball and spring model (4). The curve is constant for small $A_2 > 0$, and falls off as A_2 approaches 1, implying that random walks are unlikely to form extended structures. For $C = 0.0$–0.4, at large times, $\langle A_2 \rangle = 0.397$.

In Fig. 2, asymmetry parameters and ellipses of gyration are shown for the trajectories. These quantities are properties of the trajectory, not of the set of sites visited, so that different trajectories over the same set of points would yield different values of these quantities.

What is the probability of a fast trajectory?

To determine whether an observed trajectory is the result of directed transport or random motion, one can evaluate a_2 or A_2, and compare the measured values with the calculated probabilities. It is more convenient to do this using the cumulative probability curves of Fig. 7, calculated from the data in Figs. 5 and 6. These curves give the fraction of trajectories with an asymmetry parameter at or below a given value. For random point obstacles with $C \leq 0.4$, the cumulative curves show very little dependence on concentration (Fig. 7 *a*) or time (Fig. 7 *b*). The curves are smooth; most of the noise is averaged out. Recall that an extended trajectory corresponds to $a_2 \to 0$ and $A_2 \to 1$. Numerical values of the cumulative probability for small a_2 and large A_2 are

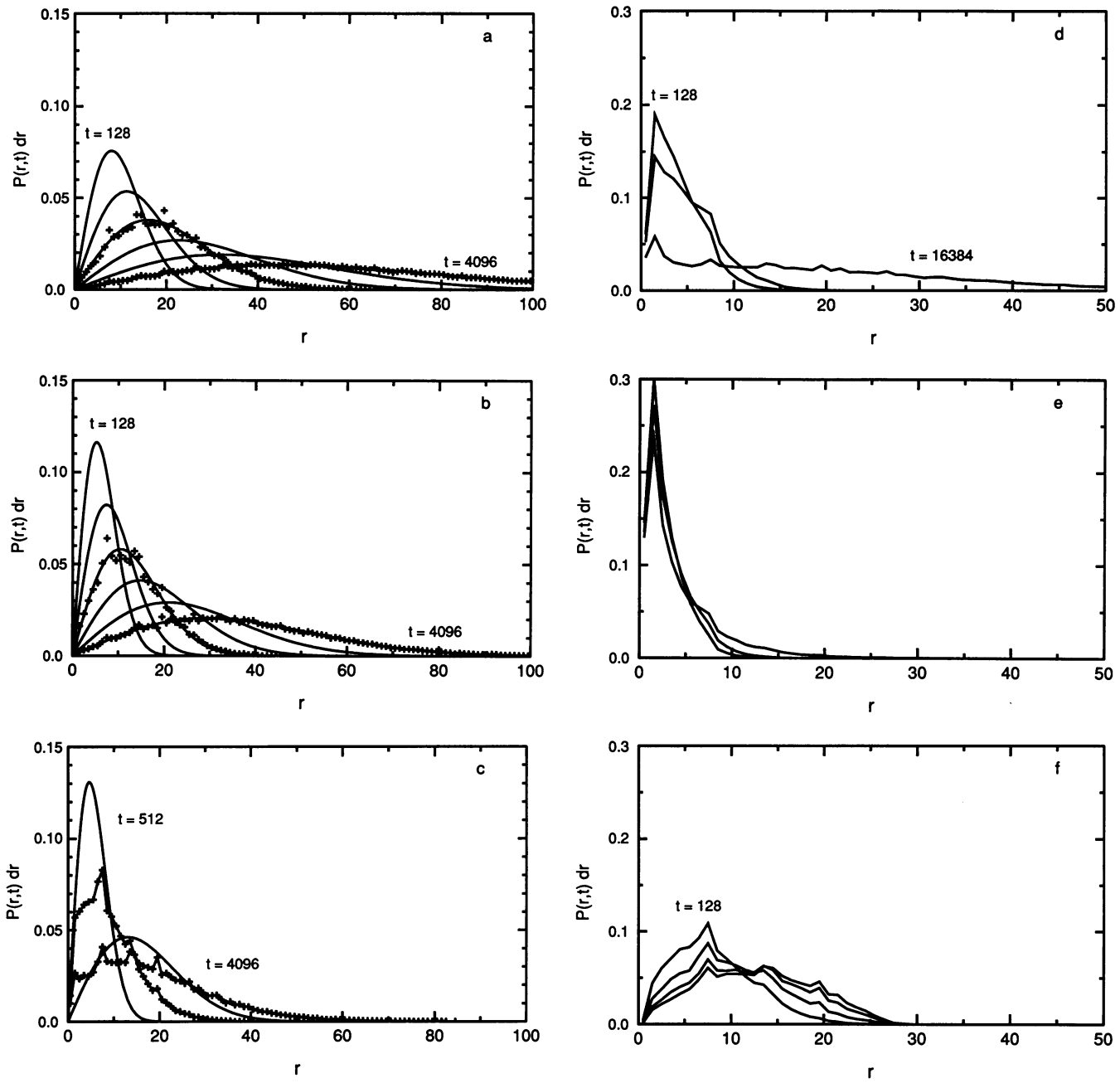

FIGURE 4 Probability density $P(r, t)dr$ from Eq. 8. Note the change of scale between the first three and the last three graphs. Histograms were calculated for $\Delta r = 0.01$. (*a*) Unobstructed diffusion, $C = 0.0$. Lines, from Eq. 8 for times $t = 128, 256, \ldots, 4096$. Crosses, Monte Carlo results for $t = 512$ and 4096. (*b*) Diffusion in presence of random point obstacles at an area fraction $C = 0.3$. Lines, from Eq. 8 for times $t = 128, 256, \ldots,$ 4096. Crosses, Monte Carlo results for $t = 512$ and 4096. Monte Carlo results for two independent runs for $C = 0.0$ and two independent runs for $C = 0.3$ were almost indistinguishable on the scale of the figure. (*c*) Crosses, Monte Carlo results for a cluster-cluster aggregate for $t = 512$ and 4096 at an area fraction $C = 0.3$. Lines, from Eq. 8. (*d*) Monte Carlo results for random point obstacles at an area fraction $C = 0.5$, the percolation threshold for site percolation on the triangular lattice, for $t = 128$, 256, and 16,384. (*e*) Monte Carlo results for random point obstacles at an area fraction $C = 0.6$, above the percolation threshold, for times $t = 128$, 256, and 16,384. (*f*) Monte Carlo results for a bounded region, a hexagon of radius 15, for times $t = 128$, 256, 512, and 16,384.

given in Table 2 (from two independent runs for $C = 0.0$, $t = 16{,}384$).

Purely linear trajectories are not a useful example of directed motion because $a_2 = 0$ and $A_2 = 1$, regardless of length. This is a limitation of the lattice model. Instead, consider a zigzag trajectory, as shown in the inset of Fig. 7 *c*. It is simple to calculate a_2 for a series of these trajectories; the fraction of random-walk trajectories at least

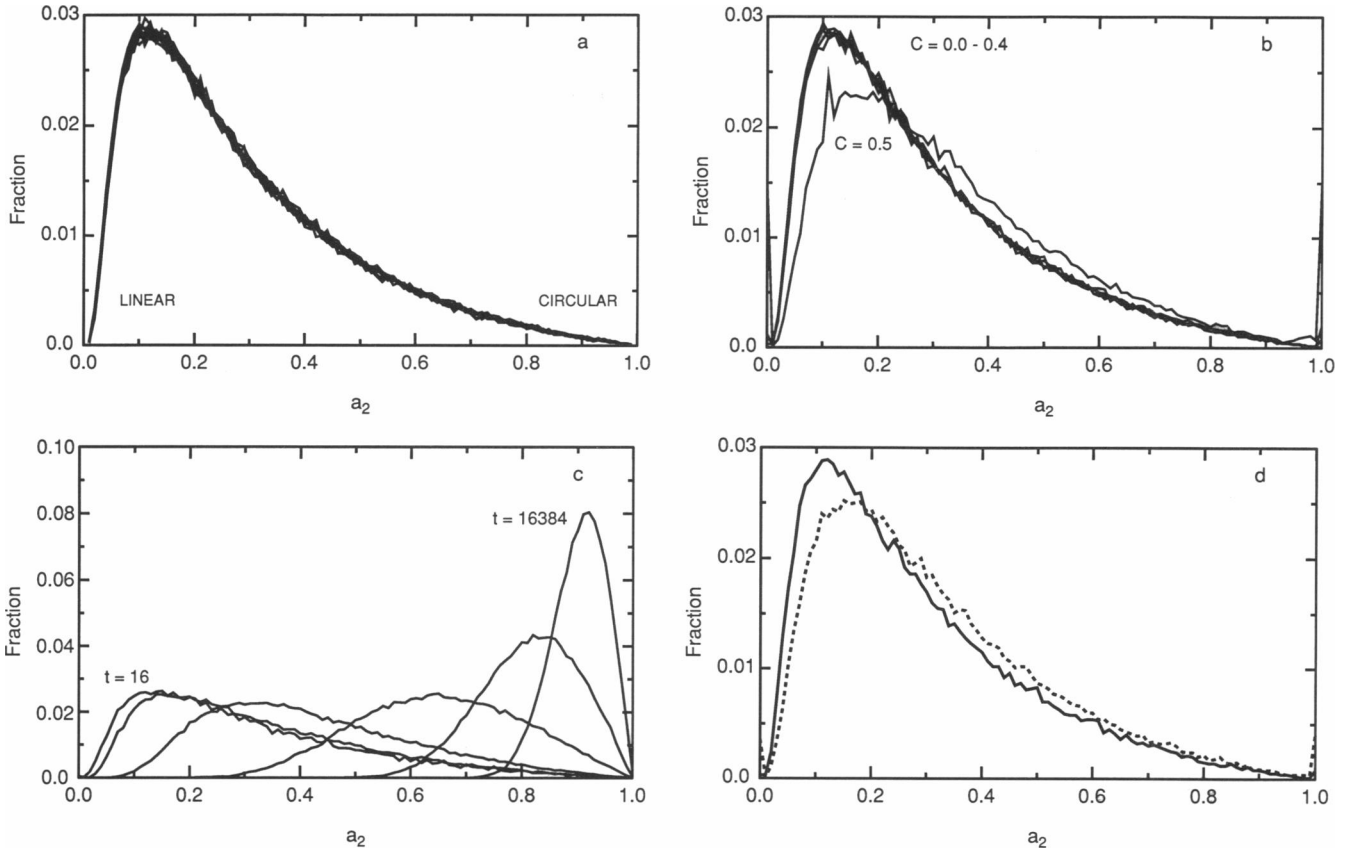

FIGURE 5 Histograms of the asymmetry parameter a_2 for random walks in the presence of various obstacles. In the histograms, $\Delta a_2 = 0.01$. (*a*) Time dependence for unobstructed diffusion. $C = 0.0$, $t = 128, 256, \ldots, 16{,}384$. Histograms for $C \leq 0.4$ show similar time dependence. The thickness of the curve is a reasonable estimate of statistical error. Curves for one independent run for $C = 0.0$ and two independent runs for $C = 0.3$ were indistinguishable from *a*. (*b*) Concentration dependence at fixed time. $C = 0.0, 0.1, \ldots, 0.5$; $t = 16{,}384$. (*c*) Time dependence of histogram for a bounded region, a hexagon of radius 7, for $t = 16, 64, \ldots, 16{,}384$. (*d*) Comparison of random point obstacles (*solid line*) and cluster-cluster aggregates (*dashed line*) at an obstacle concentration $C = 0.3$ and $t = 16{,}384$.

that elongated can then be found from Fig. 7 *a*. Values of a_2 and $\Pr(a_2)$ (interpolated from Table 2) are shown in Fig. 7 *c*, along with the probabilities from Eq. 9. Both probabilities decrease very rapidly with length. For example, a zigzag trajectory of X-displacement 12 has $a_2 = 0.0144$, and the probability that a trajectory so elongated will occur by chance in an unobstructed random walk is 0.0025 from $\Pr(r \geq r_0)$ and 0.0015 from $\Pr(a_2)$.

In testing whether an observed trajectory is likely to occur in a random walk, assume that the trajectory is random. An unobstructed random walk has no memory, so the origin of time can be chosen at will. Take $t = 0$ to be the start of the trajectory segment in question, calculate a_2 for that segment, and then determine from Fig. 7 how probable that shape of segment is in an unobstructed random walk.

What is the probability that a random walk will stay within a bounded region?

Fig. 2 shows several random walks in an unobstructed system where the tracer remains in a small region for a long time, giving the appearance that the tracer is trapped in a finite domain. To determine whether such a trajectory really indicates trapping, we need the probability $\Psi(R, t)$ that an unobstructed random walk remains within a region of radius R for all times $\leq t$. This probability is derived in Appendix A.

Fig. 8 *a* shows probability distributions from Eq. A3 and Monte Carlo results for unobstructed diffusion. Fig. 8 *b* shows similar results for diffusion in the presence of random point obstacles at an area fraction of 0.3. The small difference between the Monte Carlo results and the theoretical curves is presumably the result of lattice structure and binning into histograms. When the appropriate diffusion coefficient D^* is used, Eq. A3 can be used for $C \leq 0.3$, but as C approaches the percolation threshold, Eq. A3 no longer applies.

In Fig. 8 *c*, for a particle trapped in a hexagon of radius 7, the cumulative probability reaches a time-independent value by $t = 1024$. Fig. 8 *d* shows Monte Carlo results for a cluster-cluster aggregate at $C = 0.3$, and curves from Eq. A3 for random point obstacles at the same concentration. The two sets of curves are similar initially, but around $t = 256$, the curve for aggregates

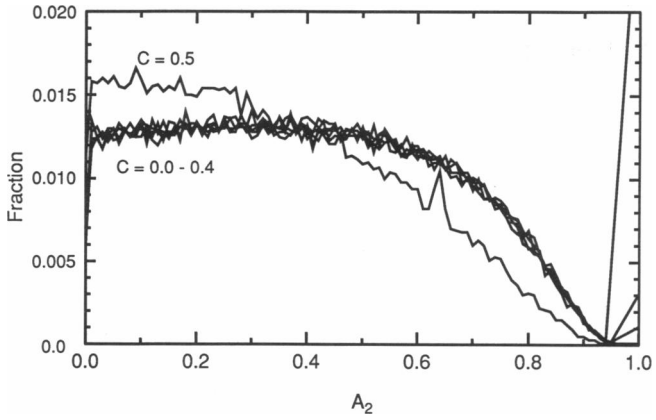

FIGURE 6 Histograms of the asymmetry parameter A_2 for random walks in the presence of various concentrations of random point obstacles, for $C = 0.0, 0.1, \ldots, 0.5$; $t = 16{,}384$. In the histograms, $\Delta A_2 = 0.01$. The peak at $A_2 = 1$ is from tracers trapped on isolated points. Again, the thickness of the curve is a reasonable error estimate.

starts to lag the curve for random point obstacles significantly. It was observed earlier that the difference between these two types of obstacles is shown most clearly in long-range diffusion measurements (42).

Suppose that a particle is observed to remain in a region $R \leq 10$. Assume $C = 0.0$, so $D^* = 1$, and Fig. 8 *a* applies. If the particle has been observed for 64 time steps, the probability that it has remained within the region $R \leq 10$ is 0.63, and one cannot tell whether the particle is trapped or not. If it remains there for $t = 256$, the probability is 0.04, suggesting trapping. If it remains there for $t = 512$, the probability is 0.0010, and trapping is likely. If random point obstacles are present at an area fraction $C = 0.3$, Fig. 8 *b* applies, and a similar argument holds, but one must observe the particle longer to conclude that it is trapped. If the particle is trapped in a hexagonal region of radius 7, Fig. 8 *c* shows that the probability is 0.25, even at long times.

This analysis can be simplified by plotting $\Psi(R, t)$ as a function of t at fixed values of R, to give the probability that a diffusing particle stays in a region R as a function of time, as shown in Fig. 9 *a*. But, according to Eq. A3, Ψ is a function of Dt/R^2 alone (or, in dimensionless variables, $D^*t^*/4R^{*2}$). So this family of curves can be plotted as a function of Dt/R^2 and reduced to a single curve, as shown in Fig. 9 *b*. For $Dt/R^2 > 0.1$, this curve is a straight line:

$$\log \Psi = 0.2048 - 2.5117(Dt/R^2). \qquad (16)$$

So, in the example of the particle in the region $R^* \leq 10$, if $D^* = 1$ and $t^* = 64$, $D^*t^*/4R^{*2} = 0.16$, and the probability $\Psi = 0.63$ can be obtained from Fig. 9 *b*. If we assume, as in the caption to Fig. 1, that $\ell = 20$ nm, $\tau_0 = 1/30$ s, and $D = 3 \times 10^{-11}$ cm^2/s, then the radius of the

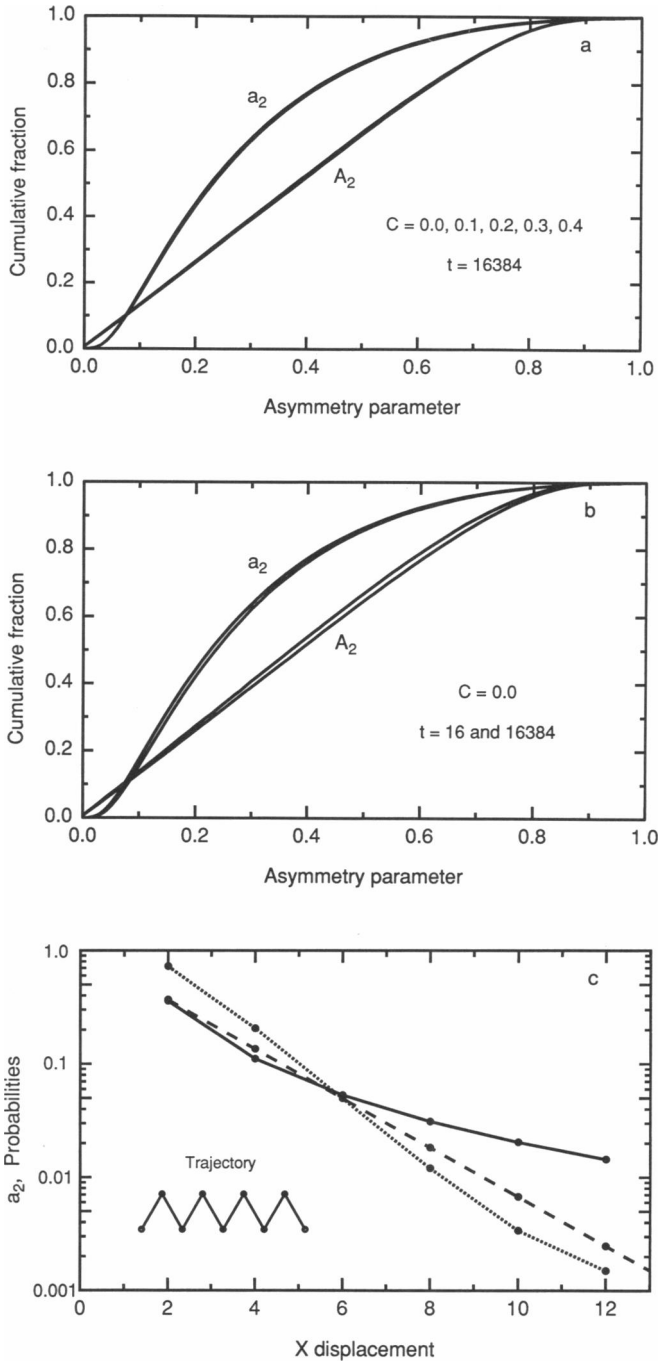

FIGURE 7 Cumulative probability curves for asymmetry parameters a_2 and A_2. (*a*) Concentration dependence. Curves are shown for random point obstacles at concentrations $C = 0.0$, 0.1, 0.2, 0.3, and 0.4, for a time $t = 16{,}384$. (*b*) Time dependence. Curves are shown for unobstructed diffusion, $C = 0.0$, for $t = 16$ and $t = 16{,}384$; intermediate times give intermediate curves. (*c*) Example. Logarithm of a_2 (*solid line*) and the probabilities $\Pr(a_2)$ (*dotted line*) from *b* and $\Pr(r \geq r_0)$ (*dashed line*) from Eq. 9 for zigzag trajectories of various lengths. The inset shows a zigzag trajectory with an X displacement of 4. The particle is assumed to move from left to right, moving one lattice constant at each time step, without retracing any of its path. For each trajectory, a_2 is calculated from Eqs. 10–14, and the probability of that value of a_2 is found from the cumulative probability curve in *b* for $C = 0.0$, $t = 16{,}384$.

TABLE 2 **Cumulative probabilities of asymmetry parameters**

a_2	$\Pr(a_2)$	A_2	$\Pr(A_2)$
0.01	0.00027	0.80	0.95865
0.02	0.00320	0.81	0.96497
0.03	0.01079	0.82	0.97067
0.04	0.02428	0.83	0.97563
0.05	0.04286	0.84	0.98027
0.06	0.06462	0.85	0.98438
0.07	0.08924	0.86	0.98794
0.08	0.11607	0.87	0.99080
0.09	0.14382	0.88	0.99316
0.10	0.17293	0.89	0.99523
0.11	0.20167	0.90	0.99682
0.12	0.23037	0.91	0.99809
0.13	0.25833	0.92	0.99889
0.14	0.28612	0.93	0.99952
0.15	0.31323	0.94	0.99981
0.16	0.33963	0.95	0.99995
0.17	0.36543	0.96	0.99999
0.18	0.39088	0.97	1.00000
0.19	0.41514	0.98	1.00000
0.20	0.43871	0.99	1.00000

region is 200 nm, $t^* = 64$ corresponds to 2.1 s, and $Dt/R^2 = 0.16$.

How long does a particle require to explore a bounded domain?

When a diffusing particle is trapped in a finite region, the mean-square displacement increases with time to a limiting value (Fig. 10 *a*)

$$\langle r^2(\infty)\rangle = 2R_G^2, \tag{17}$$

where R_G^2 is the radius of gyration of the region (32). This relation holds for both lattice and continuum diffusion.

It is more informative to show the time dependence of the mean-square displacement as a log–log plot (Fig. 10 *b*). The initial curved region then yields a straight line, and the curved transitional region is small. The initial part of the curve is given by the generalization of Eq. 1,

$$\langle r^2\rangle \propto t^{2/d_w}, \tag{18}$$

where d_w is the anomalous diffusion exponent (20). For unobstructed diffusion in a bounded region, $d_w = 2$, and the initial part of the curve is of slope 1, just as for unobstructed diffusion (Eq. 1). For random point obstacles above the percolation threshold, however, the initial slope is <1, and $d_w > 2$. This is anomalous diffusion, in which diffusion is slowed by the presence of "dangling ends, bottlenecks, and backbends" (3). Nagle (33) discusses the use of a logarithmic time scale to examine the effect of long-time tails in measurements of lateral diffusion by fluorescence photobleaching recovery.

If a diffusing particle is trapped in a circular region of radius a, the mean-square displacement $\langle r^2(t)\rangle$ can be obtained from the solution to the diffusion equation, as shown in Appendix B. In dimensionless form, this is

$$\langle r^2\rangle/\langle r^2(\infty)\rangle = 1 + F(t/\tau_0), \tag{19}$$

where $\langle r^2(\infty)\rangle$ is given by Eq. 17, $\tau_0 = \langle r^2(\infty)\rangle/D$, and the function F is defined by Eq. B14. Values of $\langle r^2(\infty)\rangle$ for some simple domain shapes are given in Eqs. B18.

This equation shows that the Monte Carlo results for unobstructed diffusion in circular regions can be reduced to a common curve by replotting the results in terms of $\langle r^2\rangle/\langle r^2(\infty)\rangle$ and t/τ_0, as shown in a log–log plot in Fig. 10 *c*. As expected, the points for diffusion in hexagonal regions follow Eq. 18 closely, as do the points for elongated hexagons of moderate elongation. For these regions $D^* = 1$, and $\langle r^2(\infty)\rangle$ was obtained from the appropriate radius of gyration of the accessible region of the lattice. For diffusion in a hexagonal region containing random point obstacles, Eq. 18 is followed for $C \le 0.2$, and deviations appear for $C = 0.3$ and 0.4. Here $D^* < 1$ was the value for a large system of random point obstacles at the prescribed concentration (Table 1).

The results for random point obstacles above the percolation threshold do not fall on the common curve. This simple scaling treatment does not apply to random point obstacles above the percolation threshold, where there is a distribution of irregularly shaped domains with irregular boundaries. The curves for $\langle r^2(t)\rangle$ are of a different form (7, 20), and this case is beyond the scope of this paper.

For particles trapped in compact regions with smooth boundaries, then, Eq. 19 can be used to estimate the observation time required for a tracer to see the boundaries of a domain of given size. The break point is at $t/\tau_0 = 1$, and the curve levels off at $t/\tau_0 = 4$. At moderate concentrations of obstacles, a diffusing particle in a finite domain reaches its limiting displacement at a time

$$t \simeq 4\langle r^2(\infty)\rangle/D. \tag{20}$$

An estimate of $t = \langle r^2\rangle/4D$ based on Eq. 1 is significantly low, even for compact regions. If the domain is very elongated, the characteristic time is greater (7).

DISCUSSION

The main point of this paper is that to interpret single-particle diffusion measurements correctly, one must consider the probability that an observed trajectory will occur, not just the trajectory itself. One must look at the statistics of random walks, just as one must use a statistical treatment to interpret single-channel conductance measurements.

A comparison of analytical and Monte Carlo results shows that for unobstructed diffusion, the analytical results apply, with $D^* = 1$, and for random point obstacles

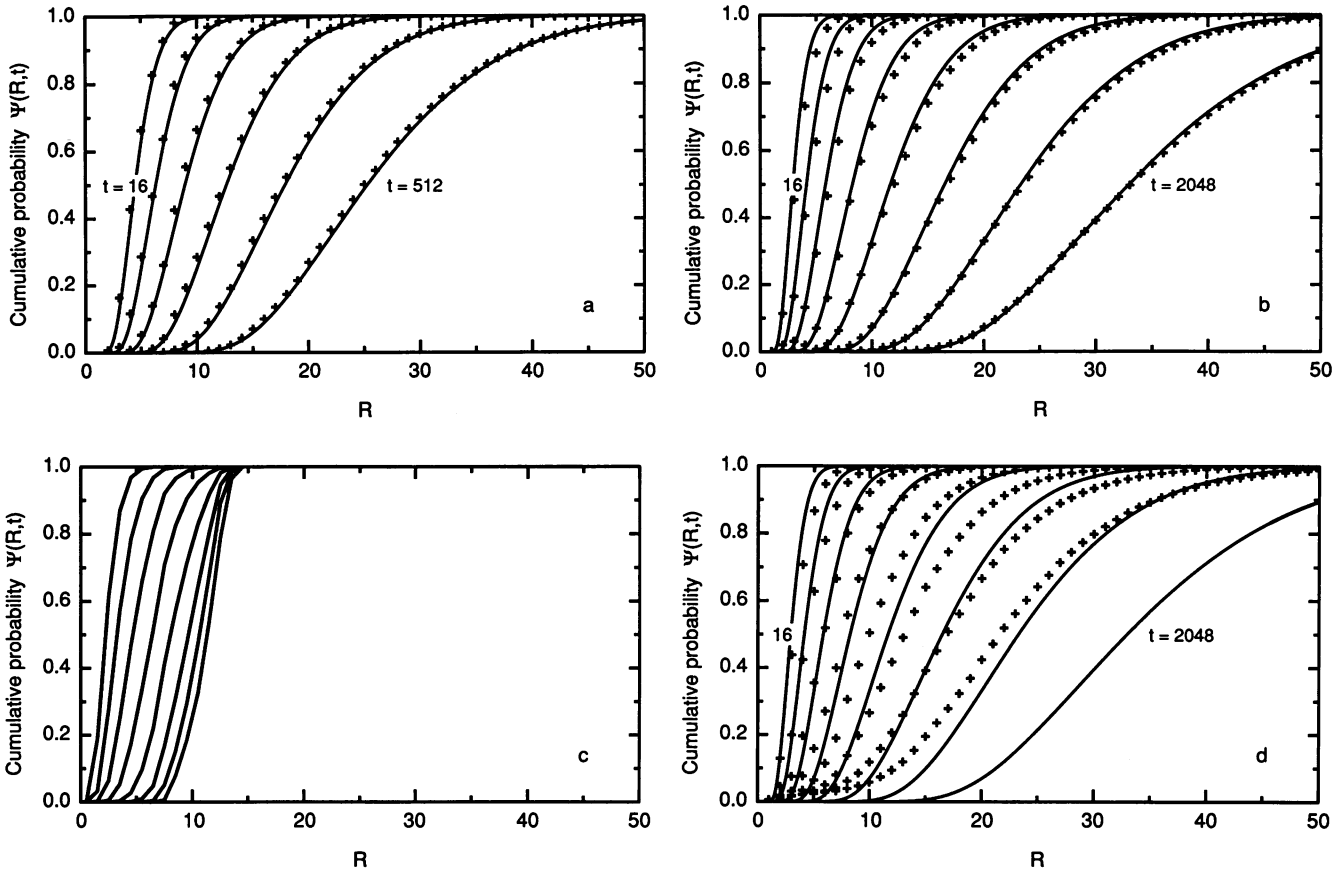

FIGURE 8 Cumulative probability $\Psi(R, t)$ that a particle remains in a region $r < R$ for all times $\leq t$, as a function of R for fixed times. (*a*) Unobstructed diffusion. Lines, from Eq. A3 for $t = 16, 32, \ldots, 512$. Crosses, Monte Carlo results for the same times. (*b*) Similar curves for diffusion in the presence of random point obstacles at an area fraction $C = 0.3$, for $t = 16, 32, \ldots, 2048$. (*c*) Monte Carlo curves for diffusion in a hexagonal region of radius 7, for times $t = 8, 16, \ldots, 512$, and 16,384. (*d*) Similar curves for diffusion in the presence of a cluster-cluster aggregate at an area fraction of 0.3 for $t = 16, 32, \ldots, 2048$. Lines, from Eq. A3, with D^* from Table 1 for random point obstacles. Crosses, Monte Carlo results.

at moderate concentrations, the analytical results still apply, but with $D^* < 1$, as Qian et al. (35) suggested. Random point obstacles simply reduce the rate of diffusion, without changing the shape of the probability distributions. So the analytical results are likely to be applicable to diffusion in most cell membranes, where the area fraction of integral protein is typically below 0.3 (reference 40, Table 1).

We have considered two biologically important limiting cases of particle motion, directed motion and trap-

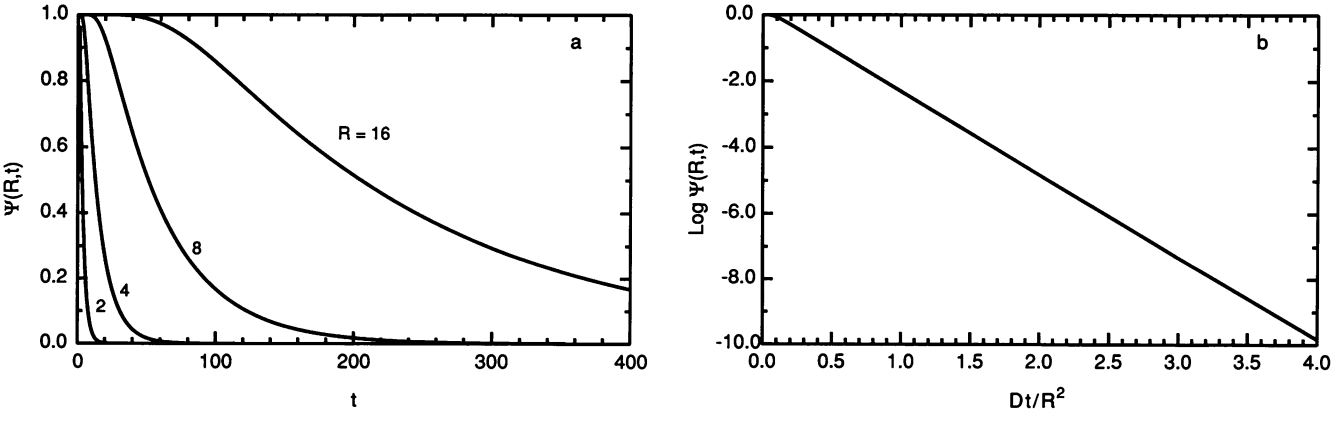

FIGURE 9 Cumulative probability $\Psi(R, t)$ that a particle remains in a region $r < R$ for all times $\leq t$. (*a*) Ψ as a function of t for unobstructed diffusion, for $R = 2, 4, 8, 16$. (*b*) Log Ψ as a function of Dt/R^2.

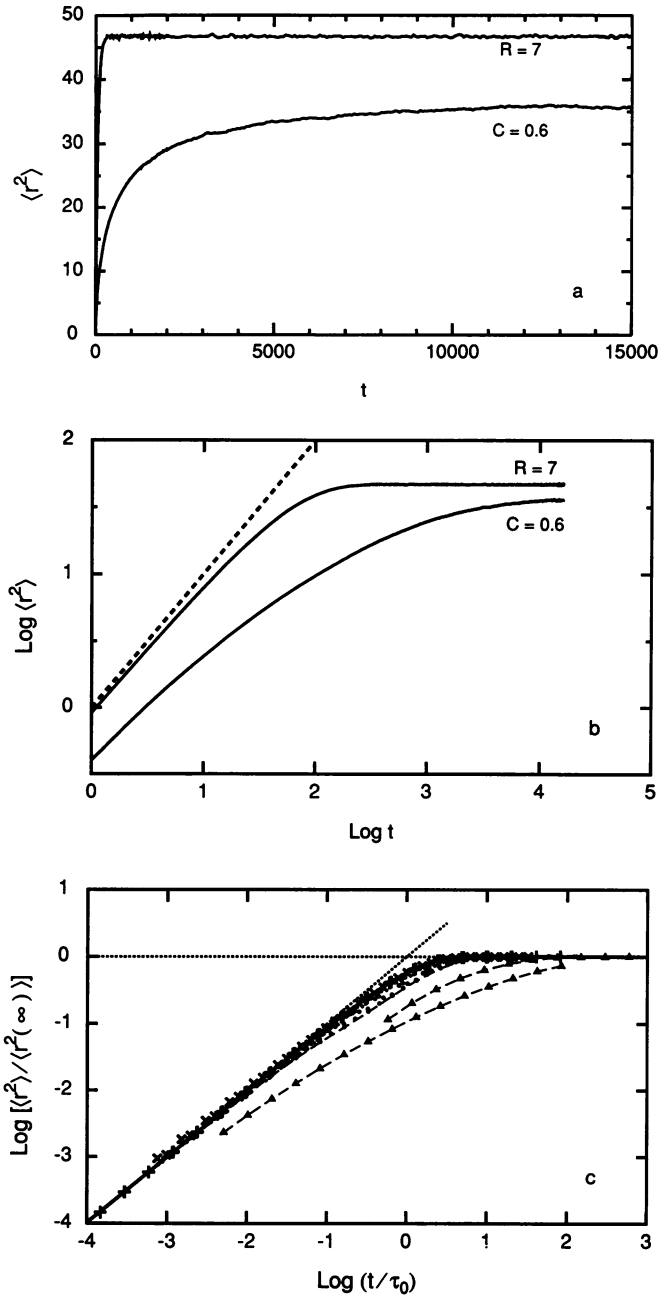

FIGURE 10 Mean-square displacement as a function of time for tracers in bounded regions. (*a*) Linear plot of $\langle r^2 \rangle$ as a function of time t (in dimensionless units), for diffusion in a hexagon of radius $R = 7$ and random point obstacles at a concentration $C = 0.6$. This is above the percolation threshold, so diffusing particles are trapped in various bounded regions. (*b*) Log–log plot of $\langle r^2 \rangle$ as a function of t for the same data. A line of unit slope is also shown. The curve for $R = 7$ shows normal diffusion ($d_w = 2$) and the curve for $C = 0.6$ shows anomalous diffusion ($d_w < 2$). (*c*) Log–log plot of scaled variables: $\langle r^2 \rangle / \langle r^2(\infty) \rangle$ as a function of t/τ_0. Solid line, Eq. 18. Dotted lines, a line of unit slope, and the line $\langle r^2 \rangle / \langle r^2(\infty) \rangle = 1$. Points, Monte Carlo results for various bounded regions, identified as follows. +, unobstructed hexagons of radius 15, 31, 63, and 127. ●, elongated hexagons of radius 7×14, 7×21, . . . , 7×49, 15×30, and 15×45. The elongated hexagons consist of 3 to 13 overlapping hexagons of radius R, with centers R lattice spacings apart along a straight line. ×, hexagons of radius 15 containing random point obstacles at area fractions of 0.1 and 0.2. ▲, random point obstacles at area fractions of 0.55 and 0.80, with $D^* = 1$. When sets of data points do not fall on the common curve, they are joined by a broken line. Deviations occur for random point obstacles, and for the most elongated hexagons; a broken line is drawn for the 7×49 elongated hexagon. Points for a hexagon of radius 15 containing random point obstacles at an area fraction of 0.3 and 0.4 are not shown, but deviate from the common curve at small t/τ_0.

ping. These cases are fundamentally different. Directed motion can be distinguished from diffusion by the shape of the trajectory, but trapping in a bounded region cannot, because we do not know the distribution of sizes and shapes of the regions. Trapping must be identified from the time dependence of properties of the trajectories.

Plotting histograms of the observed displacement at various times is a useful means of analysis, and the histograms can be fit by the theoretical curve when the obstacle concentration is below the percolation threshold. If the distribution is time independent as the observation time is varied by a factor of two or more, the tracer is likely to be trapped in a bounded domain.

For random point obstacles near or above the percolation threshold, trapping in finite regions becomes significant, and the curves for unobstructed diffusion do not apply. Such deviations might occur in chloroplasts and mitochondria.

To test for directed motion, one can use Eq. 9, or one can calculate the asymmetry parameter a_2 or A_2 for the observed trajectory, and evaluate the probability that it will occur in an unobstructed or obstructed random walk from Figs. 5 and 6.

The asymmetry parameter is not very sensitive to obstacle structure. Cluster-cluster aggregates have a much greater effect on lateral diffusion than the same area fraction of random point obstacles does, but the changes in asymmetry parameter are small, and likely to be lost in experimental noise.

To test whether a particle is trapped in a bounded region, the probability distribution of Appendix A can be used, most simply from Eq. 16. Fig. 10 *c* can be used to estimate the time required for the mean-square displacement to reach its limiting value, provided that the boundaries are smooth (nonfractal) and the region is not too elongated.

Log–log plots of the mean-square displacement as a function of time are more informative than linear plots, and might be useful for plots of experimental trajectories.

APPENDIX A

Here we obtain the probability $\Psi(R, t)$ that an unobstructed random walk remains within a given region of radius R for all times $\leq t$. This problem was solved for three-dimensional diffusion by Rubin et al. (37). The analogous derivation for the two-dimensional case is outlined here. The solution to the diffusion equation for an instantaneous source at $t = 0$, $r = 0$ in a cylindrical region of radius R with absorbing boundaries is

$$C(r, t) = \frac{1}{\pi R^2} \sum_{n=1}^{\infty} \frac{J_0(r\alpha_n)}{J_1^2(R\alpha_n)} \exp(-\alpha_n^2 Dt), \qquad \text{(A1)}$$

where J_0 and J_1 are Bessel functions and the α_n are defined by $J_0(\beta_n) = 0$, $\beta_n = R\alpha_n$ (reference 8, pp. 368–369). The fraction of random walks that remain in the region until time t is

$$\Psi(R, t) = \int_0^R C(r, t) 2\pi r \, dr, \qquad \text{(A2)}$$

so that

$$\Psi(R, t) = 2 \sum_{n=1}^{\infty} \frac{1}{\beta_n J_1(\beta_n)} \exp(-\beta_n^2 Dt/R^2). \qquad \text{(A3)}$$

The probability distribution function is $p = d\Psi/dR$, so

$$p(R, t) = (1/R)(4Dt/R^2) \times \sum_{n=1}^{\infty} \frac{\beta_n}{J_1(\beta_n)} \exp(-\beta_n^2 Dt/R^2). \qquad \text{(A4)}$$

APPENDIX B

Here we derive an expression for the mean-square displacement $\langle r^2(t) \rangle$ for a particle trapped in a circular domain of radius a.

The concentration at time t at a point (r, θ, z) due to an instantaneous point source at time 0 at $(r', \theta', 0)$ is (reference 8, pp. 376–378, Eq. 7)

$$C(r, \theta, r', \theta', t) = \frac{\exp(-z^2/4Dt)}{\pi a^2 \sqrt{4\pi Dt}} \times \left[1 + \sum_{n=-\infty}^{+\infty} \cos n(\theta - \theta') f(r, r', t) \right], \qquad \text{(B1)}$$

where

$$f(r, r', t) = \sum_{\alpha} \exp(-\alpha^2 Dt) \frac{(\alpha a)^2 J_n(\alpha r) J_n(\alpha r')}{[(\alpha a)^2 - n^2] J_n^2(\alpha a)}, \qquad \text{(B2)}$$

J_n is the Bessel function of order n, and the sum in f is over the positive roots of

$$J_n'(\alpha a) = 0. \qquad \text{(B3)}$$

The wall of the cylinder is assumed to be reflecting, so that the boundary condition is $\partial C/\partial r = 0$ at $r = a$. This is for a point source; to obtain the corresponding equation for a line source, we integrate over z, so that

$$\int_{-\infty}^{+\infty} \exp(-z^2/4Dt) \, dz = \sqrt{4\pi Dt}. \qquad \text{(B4)}$$

The concentration is normalized so that

$$\int_0^a r \, dr \int_0^{2\pi} d\theta C(r, \theta, r', \theta', t) = 1. \qquad \text{(B5)}$$

To prove this, note that the integral over θ vanishes unless $n = 0$. The integral over r of f is then proportional to (reference 1, p. 484, Eq. 11.3.20)

$$\int_0^a r \, dr J_0(\alpha r) = (a/\alpha) J_1(\alpha a). \qquad \text{(B6)}$$

But when $n = 0$, Eq. B3 implies that $J_0'(\alpha a) = -J_1(\alpha a) = 0$, so the integral over r of the series is zero, yielding Eq. B5. To find $\langle r^2(t) \rangle$, we must evaluate

$$\langle r^2(t) \rangle = \frac{1}{\pi a^2} \int_0^a r \, dr \int_0^{2\pi} d\theta \int_0^a r' \, dr' \int_0^{2\pi} d\theta' [r^2 + r'^2 - 2rr' \cos(\theta - \theta')] C(r, \theta, r', \theta', t). \qquad \text{(B7)}$$

The factor of $1/\pi a^2$ is required on account of the integration over r' and θ'. We break the integral into three terms. First,

$$I_1 = \left(\frac{1}{\pi a^2} \right)^2 \int_0^a r \, dr \int_0^{2\pi} d\theta \int_0^a r' \, dr' \int_0^{2\pi} d\theta' [r^2 + r'^2 - 2rr' \cos(\theta - \theta')] = a^2. \qquad \text{(B8)}$$

Second,

$$I_2 = \left(\frac{1}{\pi a^2} \right)^2 \int_0^a r \, dr \int_0^{2\pi} d\theta \int_0^a r' \, dr' \int_0^{2\pi} d\theta' [r^2 + r'^2] \times \sum_{n=-\infty}^{\infty} \cos n(\theta - \theta') f(r, r', t). \qquad \text{(B9)}$$

The integral over θ is zero unless $n = 0$. The r-integral can be shown to be

$$[2(\alpha a)^2 J_0(\alpha a) + (\alpha a)^3 J_1(\alpha a) - 4(\alpha a) J_1(\alpha a)]/\alpha^4$$

(reference 14, p. 333, Eq. 5; reference 13, p. 41, Eq. 72). As before, the r'-integral is proportional to $J_1(\alpha a) = 0$, so that

$$I_2 = 0. \qquad \text{(B10)}$$

Finally,

$$I_3 = (1/\pi a^2)^2 \times \int_0^a r \, dr \int_0^{2\pi} d\theta \int_0^a r' \, dr' \int_0^{2\pi} d\theta' [-2rr' \cos(\theta - \theta')] \times \sum_{n=-\infty}^{\infty} \cos n(\theta - \theta') f(r, r', t). \qquad \text{(B11)}$$

The integration over θ and θ' yields $2\pi^2(\delta_{n,-1} + \delta_{n,+1})$. The integrals over r and r' are equal:

$$\int_0^a r^2 \, dr J_1(\alpha r) = (a^2/\alpha) J_2(\alpha a) \qquad \text{(B12)}$$

(reference 1, p. 484, Eq. 11.3.20). Combining the expressions for I_1, I_2, and I_3, we obtain

$$\langle r^2(t) \rangle = a^2 \left[1 - 8 \sum_{\alpha} \exp(-D\alpha^2 t) \frac{1}{(\alpha a)^2 - 1} \frac{J_2^2(\alpha a)}{J_1^2(\alpha a)} \right]. \qquad \text{(B13)}$$

The only terms that contribute to the sum over n in I_3 are $n = \pm 1$, so that from Eq. B3, the α are defined by $J_1'(\alpha a) = 0$, or $J_0(\alpha a) = J_2(\alpha a)$ (reference 1, p. 361, Eq. 9.1.27). We use this to eliminate J_2 from Eq. B13, and substitute $\beta = \alpha a$ to obtain

$$\langle r^2(t) \rangle = a^2 \left[1 - 8 \sum_{n} \exp(-\beta_n^2 Dt/a^2) \frac{1}{\beta_n^2 - 1} \frac{J_0^2(\beta_n)}{J_1^2(\beta_n)} \right], \qquad \text{(B14)}$$

where

$$J_1'(\beta_n) = J_1'(\alpha_n a) = 0. \qquad \text{(B15)}$$

This can be rewritten in terms of the normalized mean-square displacement $\langle r^2 \rangle / \langle r^2(\infty) \rangle$ and the normalized time t/τ_0, where

$$\tau_0 = \langle r^2(\infty)\rangle / D, \tag{B16}$$

and $\langle r^2(\infty)\rangle$ is found from Eq. B18b. Then Eq. B14 can be written as

$$\langle r^2\rangle / \langle r^2(\infty)\rangle = 1 + F(t/\tau_0). \tag{B17}$$

For continuum diffusion, for a rectangular region of dimensions $2a \times 2b$,

$$\langle r^2(\infty)\rangle = {}^2/_3(a^2 + b^2); \tag{B18a}$$

for an ellipse with semi-axes a and b,

$$\langle r^2(\infty)\rangle = {}^1/_2(a^2 + b^2); \tag{B18b}$$

and for a hexagonal region of radius a,

$$\langle r^2(\infty)\rangle = {}^5/_6 a^2 \tag{B18c}$$

from standard expressions for the radius of gyration (46).

I thank J. F. Nagle for a preprint of his paper, and P. F. F. Almeida and J. E. Keizer for helpful comments.

This work was supported by National Institutes of Health grant GM-38133.

Received for publication 28 September 1992 and in final form 17 December 1992.

REFERENCES

1. Abramowitz, M., and I. A. Stegun. 1972. Handbook of Mathematical Functions. U.S. Government Printing Office, Washington, DC. 1046 pp.
2. Anderson, C. M., G. N. Georgiou, I. E. G. Morrison, G. V. W. Stevenson, and R. J. Cherry. 1992. Tracking of cell surface receptors by fluorescence digital imaging microscopy using a charge-coupled device camera. Low-density lipoprotein and influenza virus receptor mobility at 4°C. *J. Cell Sci.* 101:415–425.
3. ben-Avraham, D. 1991. Diffusion in disordered media. *Chemometrics Intelligent Lab. Syst.* 10:117–122.
4. Bishop, M., and C. J. Saltiel. 1988. Polymer shapes in two, four, and five dimensions. *J. Chem. Phys.* 88:3976–3980.
5. Bookstein, F. L. 1987. Random walk and the existence of evolutionary rates. *Palaeobiology.* 13:446–464.
6. Bookstein, F. L. 1988. Random walk and the biometrics of morphological characters. *Evol. Biol.* 23:369–398.
7. Burlatsky, S. F., A. I. Chernoutsan, and I. V. Rybalchenko. 1991. Asymptotics of random walk displacement in a percolation system under threshold. *Phys. Lett. A* 161:147–152.
8. Carslaw, H. S., and J. C. Jaeger. 1959. Conduction of Heat in Solids. 2nd ed. Clarendon Press, Oxford, UK. 510 pp.
9. de Brabander, M., R. Nuydens, A. Ishihara, B. Holifield, K. Jacobson, and H. Geerts. 1991. Lateral diffusion and retrograde movements of individual cell surface components on single motile cells observed with Nanovid microscopy. *J. Cell Biol.* 112:111–124.
10. Edidin, M. 1990. Molecular associations and membrane domains. *Curr. Top. Membr. Transp.* 36:81–96.
11. Edidin, M., S. C. Kuo, and M. P. Sheetz. 1991. Lateral movements of membrane glycoproteins restricted by dynamic cytoplasmic barriers. *Science (Wash. DC).* 254:1379–1382.
12. Eisinger, J., J. Flores, and W. P. Petersen. 1986. A milling crowd model for local and long-range obstructed lateral diffusion. *Biophys. J.* 49:987–1001.
13. Erdélyi, A., W. Magnus, F. Oberhettinger, and F. G. Tricomi. 1953. Higher Transcendental Functions. Vol 2. McGraw-Hill, New York. 396 pp.
14. Erdélyi, A., W. Magnus, F. Oberhettinger, and F. G. Tricomi. 1954. Tables of Integral Transforms. Vol 2. McGraw-Hill, New York. 451 pp.
15. Family, F., T. Vicsek, and P. Meakin. 1985. Are random fractal clusters isotropic? *Phys. Rev. Lett.* 55:641–644.
16. Feder, J. 1988. Fractals. Plenum Publishing Corp., New York. pp. 163–170.
17. Flory, P. J. 1969. Statistical Mechanics of Chain Molecules. John Wiley & Sons Inc., New York. 432 pp.
18. Ghosh, R. N., and W. W. Webb. 1987. Low density lipoprotein (LDL) receptor dynamics on cell surfaces. *Biophys. J.* 51:520*a*. (Abstr.)
19. Ghosh, R. N., and W. W. Webb. 1990. Evidence for intra-membrane constraints to cell surface LDL receptor motion. *Biophys. J.* 57:286*a*. (Abstr.)
20. Havlin, S., and D. Ben-Avraham. 1987. Diffusion in disordered media. *Adv. Phys.* 36:695–798.
21. Havlin, S., D. Movshovitz, B. Trus, and G. H. Weiss. 1985. Probability densities for the displacement of random walks on percolation clusters. *J. Phys. A.* 18:L719–L722.
22. Jacobson, K., and W. L. C. Vaz. 1992. Domains in biological membranes. *Comments Mol. Cell. Biophys.* 8:1–114.
23. Joliot, P., J. Lavergne, J., and D. Béal. 1992. Plastoquinone compartmentation in chloroplasts. I. Evidence for domains with different rates of photo-reduction. *Biochim. Biophys. Acta.* 1101:1–12.
24. Kolb, M., R. Botet, and R. Jullien. 1983. Scaling of kinetically growing clusters. *Phys. Rev. Lett.* 51:1123–1126.
25. Kucik, D. F., E. L. Elson, and M. P. Sheetz. 1990. Cell migration does not produce membrane flow. *J. Cell Biol.* 111:1617–1622.
26. Lavergne, J., and P. Joliot. 1991. Restricted diffusion in photosynthetic membranes. *Trends Biochem. Sci.* 16:129–134.
27. Lavergne, J., J.-P. Bouchaud, and P. Joliot. 1992. Plastoquinone compartmentation in chloroplasts. II. Theoretical aspects. *Biochim. Biophys. Acta.* 1101:13–22.
28. Lee, G. M., A. Ishihara, and K. A. Jacobson. 1991. Direct observation of Brownian motion of lipids in a membrane. *Proc. Natl. Acad. Sci. USA.* 88:6274–6278.
29. Mandelbrot, B. B. 1983. The Fractal Geometry of Nature. W. H. Freeman and Co., New York. 12–13.
30. Meakin, P. 1983. Formation of fractal clusters and networks by irreversible diffusion-limited aggregation. *Phys. Rev. Lett.* 51:1119–1122.
31. Mecham, R. P., L. Whitehouse, M. Hay, A. Hinek, and M. P. Sheetz. 1991. Ligand affinity of the 67-kD elastin/laminin binding protein is modulated by the protein's lectin domain: visualization of elastin/laminin-receptor complexes with gold-tagged ligands. *J. Cell Biol.* 113:187–194.
32. Mitescu, C. D., and J. Roussenq. 1983. Diffusion on percolation clusters. *Ann. Israel Phys. Soc.* 5:81–100.
33. Nagle, J. F. 1992. Long-tail kinetics in biophysics? *Biophys. J.* 63:366–370.
34. Pink, D. A. 1985. Protein lateral movement in lipid bilayers. Simulation studies of its dependence upon protein concentration. *Biochim. Biophys. Acta.* 818:200–204.
35. Qian, H., M. P. Sheetz, and E. L. Elson. 1991. Single particle tracking. Analysis of diffusion and flow in two-dimensional systems. *Biophys. J.* 60:910–921.

36. Quandt, S., and A. P. Young. 1987. The shape of two-dimensional percolation and Ising clusters. *J. Phys. A.* 20:L851–L856.

37. Rubin, R. J., J. Mazur, and G. H. Weiss. 1976. Spans of polymer chains. *Pure Appl. Chem.* 46:143–148.

38. Rudnick, J., and G. Gaspari. 1987. The shapes of random walks. *Science (Wash. DC).* 237:384–389.

39. Saxton, M. J. 1987. Lateral diffusion in an archipelago: the effect of mobile obstacles. *Biophys. J.* 52:989–997.

40. Saxton, M. J. 1989. Lateral diffusion in an archipelago: distance dependence of the diffusion coefficient. *Biophys. J.* 56:615–622.

41. Saxton, M. J. 1990. The membrane skeleton of erythrocytes: a percolation model. *Biophys. J.* 57:1167–1177.

42. Saxton, M. J. 1992. Lateral diffusion and aggregation: a Monte Carlo study. *Biophys. J.* 61:119–128.

43. Sheetz, M. P., S. Turney, H. Qian, and E. L. Elson. 1989. Nanometre-level analysis demonstrates that lipid flow does not drive membrane glycoprotein movements. *Nature (Lond.).* 340:284–288.

44. Šolc, K. 1971. Shape of a random-flight chain. *J. Chem. Phys.* 54:335–344.

45. Šolc, K., and W. H. Stockmayer. 1971. Shape of a random-flight chain. *J. Chem. Phys.* 54:2756–2757.

46. Synge, J. L., and B. A. Griffith. 1949. Principles of Mechanics. 2nd ed. McGraw-Hill, New York. 189–193.

47. Thomas, J. L., T. J. Feder, and W. W. Webb. 1992. Effects of protein concentration on IgE receptor mobility in rat basophilic leukemia cell plasma membranes. *Biophys. J.* 61:1402–1412.

48. Thompson, T. E., M. B. Sankaram, and R. L. Biltonen. 1992. Biological membrane domains: functional significance. *Comments Mol. Cell. Biophys.* 8:1–15.

49. Vaz, W. L. C. 1992. Translational diffusion in phase-separated lipid bilayer membranes. *Comments Mol. Cell. Biophys.* 8:17–36.

50. Weiss, G. H., and R. J. Rubin. 1983. Random walks: theory and selected applications. *Adv. Chem. Phys.* 52:363–505.

51. Zhang, F., B. Crise, B. Su, Y. Hou, J. K. Rose, A. Bothwell, and K. Jacobson. 1991. Lateral diffusion of membrane-spanning and glycosylphosphatidylinositol-linked proteins: toward establishing rules governing the lateral mobility of membrane proteins. *J. Cell Biol.* 115:75–84.